ELSEVIER

Polymer 43 (2002) 5949–5958

polymer

www.elsevier.com/locate/polymer

Poly(styrene-*b*-isobutylene-*b*-styrene) block copolymer ionomers (BCPI) and BCPI/silicate nanocomposites. 2. Na^+BCPI sol–gel polymerization templates

Kenneth A. Mauritz[a,*], Robson F. Storey[a], David A. Reuschle[b], Nora Beck Tan[c,1]

[a]*Department of Polymer Science, The University of Southern Mississippi, Hattiesburg, MS 39406-0076, USA*
[b]*The Dow Chemical Company, 2301 Brazosport Blvd., B-1470 Freeport, TX 77541, USA*
[c]*US Army Research Laboratory, Weapons & Materials Research, AMSRL-WM-MA/Bldg. 4600, Aberdeen Proving Grounds, Aberdeen, MD 21005-5069, USA*

Received 20 May 2002; received in revised form 20 May 2002; accepted 6 June 2002

Abstract

Polystyrene (PS) blocks in poly(styrene-*b*-isobutylene-*b*-styrene) (PS–PIB–PS) block copolymers were partially sulfonated and the acid groups converted to $Na^+SO_3^-$ groups to create ionomers. Then, dimethylacetamide was used to selectively swell the ionic PS domains and the swollen films were exposed to sol–gel reactive tetraethylorthosilicate solutions. $(EtO)_{4-x}Si(OH)_x$ monomers then permeated films so that sol–gel reactions occurred within/around the ionic PS domains. Environmental scanning electron microscopy/energy dispersive X-ray spectroscopy investigations showed that silicate structures can be incorporated within the interior of the ionomer films. Differential scanning calorimetry studies indicated that there is no variance in the PIB block T_g with respect to ionomer formation, or with respect to silicate loading of the ionomer at low levels, which suggests that the silicate component does not reside in the PIB phase. ^{23}Na solid state NMR spectroscopy detected isolated $Na^+SO_3^-$ groups as well as aggregated $SO_3^-Na^+$ ion pairs for 'as cast' and 'dry' non-silicate containing ionomer samples. In a hydrated sample, almost all Na^+ ions were solvent-separated. AFM analysis showed that phase separation exists, but that the degree of order is significantly less than that for hybrids based on the corresponding benzyltrimethylammonium ionomer. This frustrated morphology was also seen in the results of small angle X-ray scattering experiments. Given the scale of organic/inorganic heterogeneity, these hybrids are properly classified as nanocomposites.

Keywords: Block copolymer ionomer template; In situ sol–gel reactions; Ionomer/silicate nanocomposite

1. Introduction

Mauritz et al. [1–7] created a variety of (organic polymer)/(inorganic oxide) hybrid materials via polymer in situ sol–gel polymerizations of metal alkoxide and organo-alkoxysilane monomers. In one case, it was demonstrated that the quasi-ordered, phase-separated morphology of Nafion® perfluorosulfonate ionomer membranes can serve as a 3D template for these polymerizations [1]. 'Template', in this context, refers to the targeted growth of inorganic oxide or organically modified silicate structures within a specific nanostructured polymer phase based on the energetic affinity of the alkoxide monomer, or more often its hydrolyzed versions, for this phase. In the case of Nafion® membranes, it appears that the sol–gel reactions of sorbed, hydrolyzed silicon alkoxides are confined to the sulfonate-terminated sidechain aggregate domains wherein silicate or organically modified silicate particles are formed [8].

In a more recent study aimed at testing the template concept for different polymer morphologies, silicate structures were successfully inserted within the rod-like hard block domains in a benzyltrimethylammonium ($BTMA^+$) ionomer form of sulfonated poly(styrene-*b*-isobutylene-*b*-styrene) (PS–PIB–PS) tri-block copolymers via in situ sol–gel reactions for tetraethylorthosilicate (TEOS) [9]. The combination of a PS domain-selective swelling agent, namely dimethylacetamide (DMAc), and attachment of the large organic counterion ($BTMA^+$) along the styrene blocks facilitated preferential migration of hydrolyzed $Si(OEt)_4$ monomers to these ionic domains wherein the sol–gel reactions were seeded, as crudely depicted in Fig. 1. Differential scanning calorimetry (DSC) and dynamic mechanical studies indicated that T_g for the PIB phase is

* Corresponding author.
[1] Present address: W.L. Gore & Associates, 501 Vieve's Way, Elkton, MD 21922, USA.

0032-3861/02/$ - see front matter
PII: S0032-3861(02)00387-7

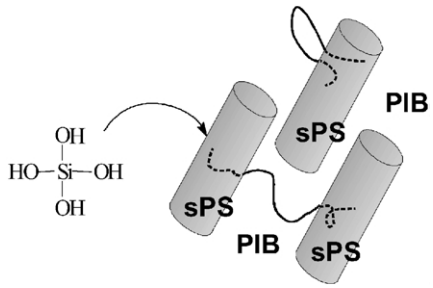

Fig. 1. Depiction of PS domain—targeted silicate formation via BCPI—in situ sol–gel reactions for hydrolyzed TEOS. The sPS domains have attached cation-sulfonate groups.

essentially unaffected by PS block sulfonation and neutralization of sulfonic acid groups by $BTMA^+$ cations, as well as by subsequent composite formation via an in situ sol–gel process for TEOS. On the other hand, the PS phase T_g shifted to higher values with ionomer formation, and to higher values with subsequent silicate phase insertion. The general conclusion was that the silicate component was incorporated in the PS rather than in the PIB domains. These thermal analysis results, when combined with the results of earlier atomic force microscopy (AFM) [10] and small angle X-ray scattering (SAXS) [11] investigations, demonstrated that the basic rod-like morphology of the unmodified block copolymer (BCP) remains unchanged despite insertion of a silicate phase. Thus, the concept of a robust sol–gel reaction template was reinforced in that the phase-separated morphology of the unfilled ionomer is preserved despite its invasion by the in situ-grown, sol–gel-derived silicate component.

In a somewhat similar study, Chen et al. [12] created elastomeric four-arm star poly(styrene–butadiene) (PS–PB) BCP/silicate hybrid materials via a sol–gel process wherein films were cast from a solution of PS–PB, TEOS, water, and tetrahydrofuran (THF). Dynamic mechanical analysis showed an invariance of T_g for the butadiene blocks after modification, and the results suggested that the silicate component preferentially formed in the PS outer blocks whose T_g increased with increasing silicate content.

Our studies were extended with investigations aimed at determining whether the Na^+ form of the same sulfonated PS–PIB–PS BCP ionomers (BCPI) would likewise act as a sol–gel polymerization template and whether there would be differences in the geometrical dispersion of the silicate component. The compatibility of hydrolyzed TEOS monomers with the PS domains and degree of swelling of these domains using a particular solvent would depend on the nature of the monovalent cation on the basis of size and organic vs. inorganic character.

The PS blocks in the same elastomeric PS–PIB–PS BCPs that have cylindrical morphologies were sulfonated and the sulfonic acid groups were converted to $Na^+SO_3^-$ ion exchange groups. DMAc was again used to selectively swell the ionic PS domains. DMAc-swollen films were immersed in sol–gel reactive TEOS solutions during which time polar $(EtO)_{4-x}Si(OH)_x$ monomers diffused into ionic PS regions where the condensation reactions that are seen in the following scheme take place:

$$\equiv Si-OR + H_2O \underset{\text{Esterification}}{\overset{\text{Hydrolysis}}{\rightleftharpoons}} \equiv Si-OH + ROH$$

$$\equiv Si-OR + HO-Si\equiv \underset{\text{Alcoholysis}}{\overset{\text{Alchol condensation}}{\rightleftharpoons}} \equiv Si-O-Si\equiv + ROH$$

$$\equiv Si-OH + HO-Si\equiv \underset{\text{Hydrolysis}}{\overset{\text{Water condensation}}{\rightleftharpoons}} \equiv Si-O-Si\equiv + H_2O$$

Silicic acid oligomers, and later, extended gel-like structures will form. These solvent-imbibed structures further condense and solidify upon sample drying. The main factors affecting sol–gel reactions and resultant amorphous silicate structures are the mole ratio $H_2O/SiOR$, pH, reaction time, temperature, and drying conditions imposed beyond the gel point [13]. However, when sol–gel reactions take place within a polymer medium, the influence of these variables can be altered or complicated by interactions and diffusion limitations posed by the polymer matrix, especially within phase separated polymers. One of the interactions in the BCPI systems of interest is posed by the sulfonate-associated counterions. In Part 1, of this work [9], the large complex $BTMA^+$ counterion had a low surface charge density and contained organic benzyl and methyl groups. In the studies reported here, the alkali metal counterion Na^+ is much smaller and has a high surface charge density. Thus, Coulombic forces acting on polar $(EtO)_{4-x}Si(OH)_x$ monomers that migrate to the functionalized PS domains will be stronger for Na^+ than for the $BTMA^+$ counterions. This, in turn, might cause nanocomposite morphologies for the two cases to be different.

The details of the preparation of these nanocomposites and results of their characterization using environmental scanning electron microscopy/energy dispersive X-ray spectroscopy (ESEM/EDS), DSC, AFM, SAXS, and ^{29}Si solid state NMR (SSNMR) spectroscopy are reported here.

2. Experimental

2.1. Block copolymer synthesis

The linear poly(styrene-*co*-isobutylene-*co*-styrene) triblock copolymers were synthesized by a sequential living cationic polymerization by Storey, as described earlier [14–16]. Absolute molecular weight and molecular weight distribution of the PIB middle block as well as the entire BCP were determined by the use of gel permeation chromatography (GPC) in conjunction with on-line multi-angle laser light scattering (MALLS) detection. The GPC system consisted of an Alcott model 728 autosampler, a Waters model 510 solvent delivery system, a Waters model 410 differential refractometer, a Waters model 484 tunable

ultraviolet detector that was operating at 256 nm, a Wyatt Technology miniDAWN® on-line MALLS detector and two Polymer Laboratories mixed-D columns (pore-size range 50–10^4 Å, 5 μm bead size) that were thermostated to 30 °C. THF, freshly distilled from CaH_2, was employed as the mobile phase and was delivered at a flow rate of 1.0 ml/min. Sample concentrations were approximately 4 mg/ml with an injection loop volume of 110 μl. Detector signals were simultaneously recorded and absolute molecular weights and polydispersity indices (PDIs) were calculated using ASTRA™ software (Wyatt Technology Inc.). The value of d*n*/d*c* was calculated by the software using the signal from the differential refractometer and assuming 100% mass recovery from the columns.

^{1}H NMR spectroscopy was used to measure the PS weight fraction by comparing the integrated areas under the aliphatic and aromatic regions of the spectra as described previously [16]. The PS volume fraction was calculated for the BCP using the densities 1.06 and 0.92 g/cm^3 for PS and PIB, respectively. Spectra were obtained using a 200 MHz Bruker NMR spectrometer. Samples were analyzed as 10% (w/v) solutions in $CDCl_3$, using tetramethylsilane as an internal reference.

The molecular weights, PDIs, and styrene compositions of the BCPs used in these experiments are listed throughout the text for each experimental investigation. All of the similar BCP compositions are in a range corresponding to morphologies consisting of PS rods in a continuous PIB phase.

2.2. Styrene block sulfonation

Sulfonation of the BCP PS blocks was carried out using acetyl sulfate as sulfonating reagent using a method that was adapted from that of Weiss et al. [17]. Acetyl sulfate was generated by mixing an excess quantity of acetic anhydride with sulfuric acid. 7.6 ml of acetic anhydride was added to 40 ml dichloroethane (DCE) and this mixture was chilled using an ice water bath. 2.8 ml of concentrated sulfuric acid was then added to the DCE/acetic anhydride solution. The reagent was mixed in the ice bath and the solution removed from the bath and covered with paraffin film until used. A solution prepared in this manner contains ~1 M acetyl sulfate and the reagent is 'fresh' and active for about 2 h. The sulfuric acid was about 95% pure with water being the remaining 5% impurity. As water destroys acetic anhydride, the latter was added in excess of 1:1 mol/mol with sulfuric acid.

The sulfonating reagent was added through the nitrogen purge inlet of a 500 ml round-bottomed flask reactor and the purge discontinued upon addition of reagent and the purge line replaced with a ground glass stopper. The parent BCP was dissolved in DCE and this solution heated to 50 °C; the reactor was kept at this temperature for the duration of the sulfonation reaction.

As water and other protic solvents degrade acetic anhydride as well as acetyl sulfate, alcohol was added to the reactor after 2 h to terminate the reaction and the heating mantle turned off. The solution was then transferred to a separatory funnel and steam stripped (flash precipitated) into stirred boiling water.

Sulfonated polymer crumb was isolated from water when it had cooled and then transferred to a large beaker containing clean, de-ionized water and then heated. The crumb resided in hot water for several hours to leach out residual sulfuric acid. The crumb was then isolated from water and dried in vacuum at room temperature.

Mole percent sulfonation was determined by titration with standardized methanolic sodium hydroxide. The sBCP was dissolved into equal amounts of methylene chloride and hexane and a small amount of methanol added. Phenolphthalein was added to the sBCP solution and base added dropwise. Titration of a 'blank' solution accounted for the influence of solvent on the indicator.

An alternative titrimetric method involved dissolving the sBCP in chloroform containing a small amount of methanol, using phenolphthalein as indicator. The base, 0.01 M methanolic sodium hydroxide, was standardized against either *para*-toluenesulfonic acid (*p*TSA) or benzoic acid. The solvent for base standardization is the same as that for sBCP dissolution/titration. *p*TSA would seem to be a better model for sPS, but it was seen that the results were essentially the same as for benzoic acid.

2.3. Na^+ ionomer formation

Conversion of the sBCP to the Na^+ form was affected at 80 °C by the titration of a solution of tetrachloroethylene and hexanol and the sulfonic acid functionalized BCP via addition of methanolic sodium hydroxide. In all cases, 100% neutralization was achieved and the films were cast onto the surfaces of Teflon® pans. The films were dried and annealed at an elevated temperature under vacuum.

It was demonstrated by means of ESEM/EDS that most, if not all of the silicate component exists in the form of surface-attached layers on the acid form BCP films when these films were immersed in TEOS sol–gel reaction baths so that these samples are not true composites. For this reason, only the ionomer forms were used in nanocomposite formation.

2.4. Na^+BCPI in situ sol–gel reactions and Na^+BCPI/silicate hybrid materials

Typical sol–gel reaction conditions were as follows: a Na^+BCPI film was swollen in DMAc to have a weight gain of around 100%. A solution of 80 ml DMAc, 64 ml TEOS and 20 ml acidified water (pH ~ 1.2) was prepared in a separate flask and swirled until it appeared homogeneous. The solvent-swollen BCPI film was then placed in the sol–gel reactor for several minutes. The films were swirled in the sol–gel reactor to keep fresh solution in contact with its

surface. Afterward, the films were removed, rinsed with absolute ethanol to remove possible surface precipitates, blotted, and then placed on a non-stick surface. Then, the sample was transferred to a vacuum oven at 100 °C to remove solvent and further drive condensation reactions between residual SiOH groups; this temperature was maintained for one day. After this, the temperature was raised to, and held at 120 °C for one day. Finally, the temperature was raised to 160 °C for ~6 h to remove residual solvent from the film. The vacuum oven was then allowed to cool to room temperature, after which the films were removed for analysis. The mass of the BCPI film was determined by gravimetric means before and after the in situ sol–gel reaction followed by film drying. Weight percent uptake was calculated as [(composite mass − unfilled BCPI mass)/unfilled BCPI mass] × 100%.

2.5. Environmental scanning electron microscopy/energy dispersive X-ray spectroscopy

An ElectroScan E20 ESEM instrument with a Tracor-Noran Series II EDS system was used to inspect surfaces and cross-sections of BCPI/silicate films to obtain silicate concentration profiles. Fresh cross-sections for these samples were generated by cryo-microtoming using a diamond knife. Owing to the magnitude of typical hemispherical sample-beam interaction volumes for back-scattered electrons and X-rays (several microns) the spots analyzed by EDS along a line perpendicular to the film surface were separated by tens of microns. The Si/S X-ray count ratio normalizes the quantity of Si to the number of $-SO_3^-$ groups at a given point and this ratio vs. depth into the film is referred to as a Si compositional profile. Although the results should be viewed as semi-quantitative, it is stressed that the main goal was to determine whether silicate structures have primarily formed within the bulk of the film. The primary objective of these experiments was to ascertain whether sol–gel reactions for TEOS did in fact occur within the bulk of the film as opposed to the undesirable condition where a pure silica layer precipitates on the film surface.

2.6. Differential scanning calorimetry

DSC experiments were conducted using a Mettler thermal analysis work station. Data were collected with a DSC 30 and TC 15 controller. First and second heating scans were run from − 150 to 200 °C at 10 °C/min although the thermograms are displayed over a smaller range to focus on the transitions of interest. All the samples were cooled at the rate of − 10 °C/min. T_g is taken as the maximum on the first derivative DSC curve (inflection point).

Scans were obtained for the parent BCP, a corresponding BCPI, and Na^+BCPI/silicate composites having 1.88 and 3.44 wt% silicate. A control sample consisted of an unmodified BCP having the same molecular weight and PS content as the modified samples. Also, a DSC scan was obtained for a case in which the parent BCP was swollen with DMAc and then dried in vacuum to investigate whether the BCP morphology might be altered by solvent-induced molecular rearrangements. All samples were taken from the same film.

2.7. ^{23}Na solid state NMR spectroscopic studies

^{23}Na SSNMR spectra were obtained using a Bruker MSL-400 instrument operating at 105.8 MHz. The external reference of NaCl (crystalline solid), which has a chemical shift of 7.1 ppm relative to the standard NaCl aqueous solution, was used to set the frequency axis. All solid samples were run in zirconia rotors using magic-angle spinning (typically at 5 kHz) and high-power proton decoupling. To achieve uniform excitation, samples were run with a pulse width of 1.5–2.0 μs. A pulse delay of 10 s was used to obtain fully relaxed spectra.

A Na^+ form BCPI having no incorporated silicate was investigated. The particular BCP that was analyzed had $M_w = 78\,400$ g mol^{-1} and 28.5 mol% PS, of which 12.8% is sulfonated.

Three types of samples were tested. An ‘as cast’ sample was prepared by film casting and allowed to sit on the bench top as exposed to ambient air and humidity. A ‘dry’ sample refers to an as cast film, but which was placed in a vacuum oven at 100 °C for 4 days, and subsequently stored in a desiccator. A ‘hydrated’ sample was a BCPI film that was first subjected to boiling water and then remained in contact with water in a room temperature storage condition. The BCPI film was estimated to swell to ca. 2.3 wt% in water, which corresponds to about 36 moles of water per mole of sodium sulfonate groups.

2.8. Atomic force microscopy

Tapping mode AFM collected information about the sample surface. Tapping mode/phase imaging yields information related to the distribution of local viscoelastic properties across the surface. Within the context of the materials of interest here, the hard PS domains will give a different phase response than the rubbery PIB domains and the phase difference will be even greater if a hard silicate phase is incorporated in/around the PS domains.

A small film sample was sectioned with a microtome using a diamond knife below the PIB phase glass transition (− 120 °C). The block face obtained by sectioning was flat, and well suited for AFM analysis. A film piece was mounted edgewise onto a metal stub. Smoothing of the block face was done using a microtome and this block face was analyzed by tapping mode/phase AFM.

A Digital Instruments D3000 AFM was used to collect the images. Accompanying software and hardware was used for data acquisition. An untreated 125 μm silicon probe tip cantilever was used. All experiments were carried out at room temperature under ambient humidity.

2.9. Small angle X-ray scattering

SAXS data were gathered for the purpose of complementing morphological information obtained by AFM. The position and number of peaks on scattered intensity vs. scattering vector profiles can give information on the nature and degree of long range order and characteristic spacing between structural elements based on electron density contrast. Data were collected using the National Synchrotron Light Source at Brookhaven National Laboratory. Two-dimensional X-ray patterns were collected using a pinhole collimated beam and image plate detectors. Patterns were corrected for background and converted to 1D data by circular averaging.

The parent BCP used in the analysis had $M_w = 78.4$ kg mol^{-1} and 28.5 wt% PS of which 12.8 mol% was sulfonated. Samples consisted of pieces of solvent cast BCPI films that were cut to the dimensions of ca. 1 cm × 1 cm. Nominal film thickness was 1.0 mm. Plots of log scattered intensity vs. scattering vector q were constructed. Bragg spacings, d, were obtained from the values of q corresponding to intensity peaks using the equation $d = 2\pi/q$.

3. Results and discussion

3.1. Silicate uptake by Na^+BCPI films

A representative Na^+BCPI film sample, having $M_w = 78.4$ kg mol^{-1} with PDI = 1.25 and 28.5 wt% PS, which was sulfonated to the extent of 12.8 mol%, for example, will absorb DMAc in monotonic fashion to 205 wt% in 480 min. The silicate uptake for this sample monotonically increases with increased degree of pre-swelling, as shown in Fig. 2.

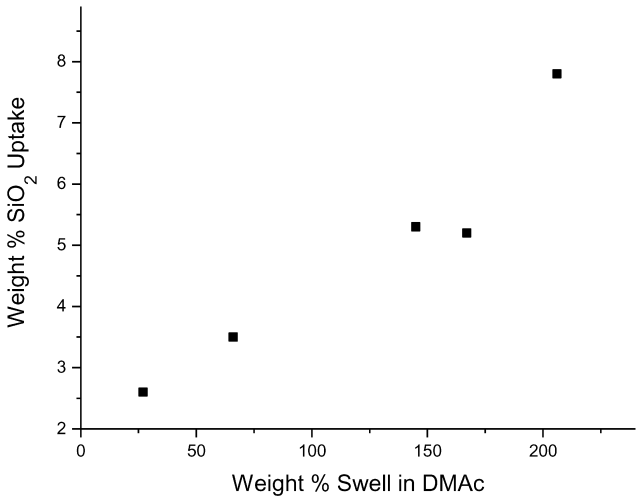

Fig. 2. Silicate weight percent uptake as a function of the degree of film swelling in DMAc prior to the in situ sol–gel reaction for sorbed TEOS. In this case, the swollen Na^+BCPI films were immersed in TEOS solution for 10 min.

3.2. ESEM/EDS Studies of Si/S compositional profiles

Two Na^+BCPI/silicate composite films were prepared for these investigations. One was based on a parent BCP for which $M_w = 71.4$ kg mol^{-1}, with 24.9 wt% PS of which 19.2 mol% was sulfonated. This sample was ~0.1 mm thick and had a silicate uptake of 5.7 wt%. Fig. 3 is a typical micrograph of this sample. Particulate debris is seen on the surface and cross-section, but this is believed to arise in the course of sample handling. It is also seen that the Si/S composition profile is very uniform across the entire thickness direction.

It appears that, for samples of this thickness, the limitation on the sol–gel reaction posed by the inward diffusion of the $(EtO)_{4-x}Si(OH)_x$ monomers is not so great as to prevent silicate structures from forming at the center of the film within the time frame of the experiment.

Another Na^+BCPI/silicate composite was made from a thicker film (~1 mm). The parent BCP for this series had $M_w = 78.4$ kg mol^{-1} and 28.5 mol% PS of which

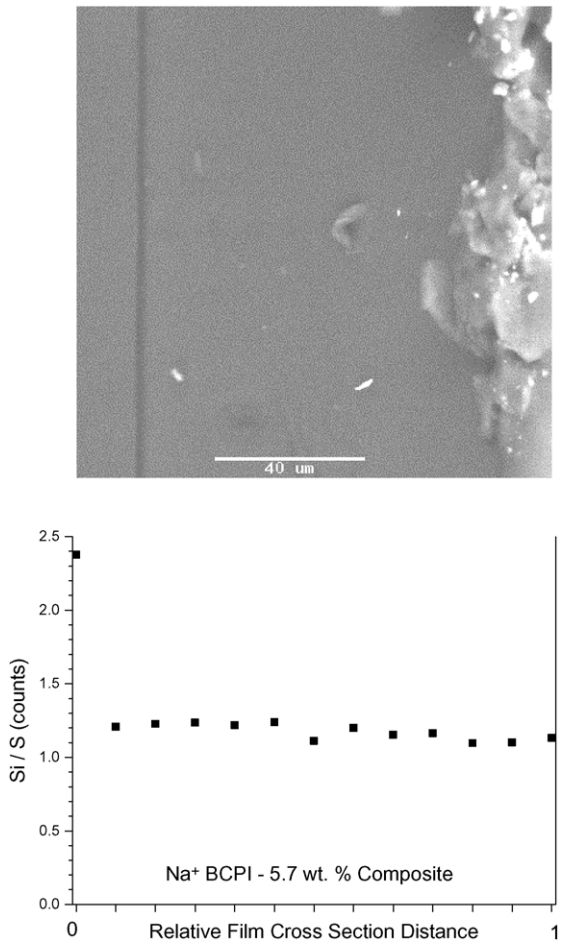

Fig. 3. Bottom: EDS Si/S relative composition profile across the thickness direction of a film for a composite having 5.7% silicate. The film is ~0.1 mm thick. The positions 0 and 1 on the horizontal axis correspond to the two film surfaces. Top: cross-section of the same sample as viewed by ESEM.

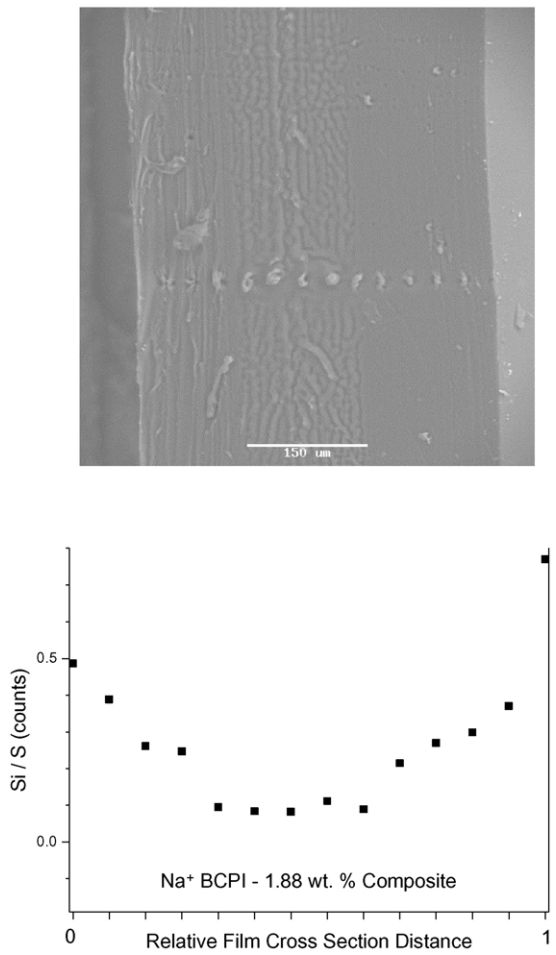

Fig. 4. Bottom: EDS Si/S relative composition profile across the thickness direction of a film for a composite having 1.88 wt% silicate, that is ~1.0 mm thick. The positions 0 and 1 on the horizontal axis correspond to the two film surfaces. Top: cross-section of the same sample as viewed by ESEM.

12.8 mol% was sulfonated. The silicate uptake of this film was 1.88 wt%. These thicker samples were cut with a clean razor blade to reveal a cross-sectional surface. Contrasted with Fig. 3, the Si/S relative composition profile seen in Fig. 4 has the shape of a trough rather than a horizontal line. There is greater silicate loading in the near surface regions than in the interior. Fig. 4 indicates no gross silica precipitation on the film surface so that all of the 1.88 wt% uptake occurred within the BCPI film. Beam damage is seen where the electron beam is directed for each point sampled on the surface.

In composite preparation, TEOS permeation time is the same for the two samples (10 min). The trough shape of the Si/S composition profile for the case in Fig. 4 reflects the fact that the film is around 10 times thicker than that for the previous case. Since the sol–gel reaction is diffusion controlled, especially in a polymer medium, a significant concentration of silicate structures have not accumulated in the film center within the experimental time frame.

Fig. 5 shows the morphology and Si/S composition profile across the thickness of a composite that incorporates 3.44 wt% silicate. There is no gross silica precipitation on the film surfaces. The parent BCP in this case is the same as that for the prior-discussed composite that had 1.88 wt% silicate and these films were also immersed in the sol–gel reactive solution for 10 min. The larger net uptake is caused by the fact that the BCPI film for the composite with 3.44 wt% silicate was pre-swollen in DMAc to a larger extent. The relative silicon counts in the near surface regions are significantly higher than Si/S toward the middle of the film. Moreover, there is a sharp drop in Si/S at about 1/3 of the distance from the surfaces. Given the greater propensity for TEOS sorption owing to greater BCPI pre-swelling, perhaps silicate structures grow to such a degree so as to block further diffusion of silicate monomers to the center of the film in this case.

It is seen in Fig. 5 that there is beam damage at points on the surface of the 3.44 wt% silicate composite at points where EDS detected low Si concentration. In other

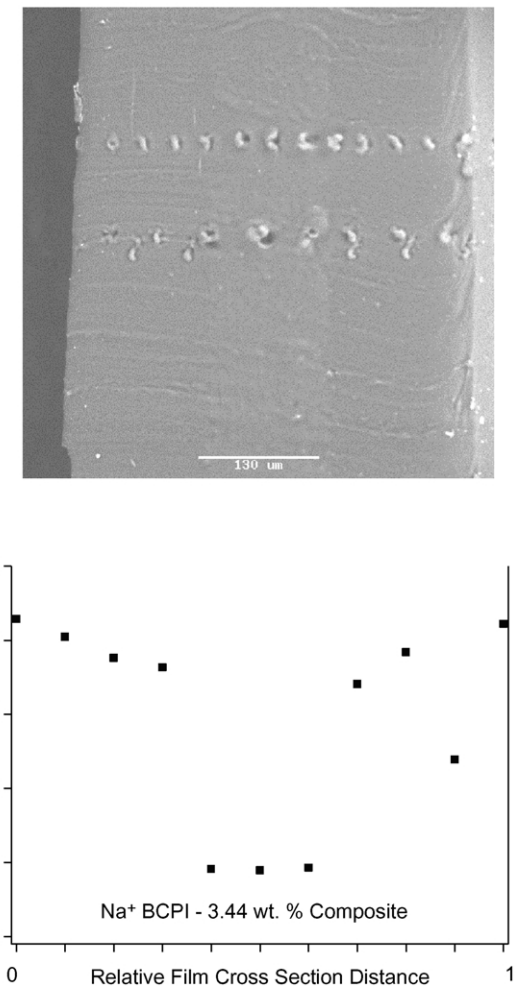

Fig. 5. Bottom: EDS Si/S relative composition profile across the thickness direction of a film for a composite sample having 3.44 wt% silicate. The sample is ~1.0 mm thick and the positions 0 and 1 on the horizontal axis correspond to the two film surfaces. Top: cross-section of the same sample as viewed by ESEM.

experiments, micrographs were generated for different times during which the film was exposed to the electron beam during imaging (1, 2, and 6 min). Good correlation exists between visual beam damage location and data point location on the EDS profile; in short, the heaviest beam damage occurs where silicate loading is the lowest.

It is stressed that the results of these ESEM–EDS experiments should be viewed semi-quantitatively. Nonetheless, it is clear—and this was the main objective of these experiments—that it is possible to incorporate silicate structures within Na^+BCPI films and that the inorganic composition profile depends on sample thickness.

3.3. DSC studies of glass transition behavior

Second scan DSC thermograms for the unmodified BCP control, a DMAc-swollen/dried BCP, a Na^+BCPI, and two Na^+BCPI/silicate composites are shown in Fig. 6. The parent BCP has $M_w = 78.4\ kg\ mol^{-1}$ and contains 28.5 wt% PS of which 12.8 mol% is sulfonated. The glass transition for the PIB phase is rather distinctive in all of the variants. A feature in the region corresponding to pure PS (~100 °C) is not apparent, although glass transitions that are weak or invisible on DSC traces are often seen using dynamic mechanical analysis. This was indeed the case for the $BTMA^+$ cation form and silicate containing nanocomposites derived from this same BCPI [9].

As in the case of the $BTMA^+$BCPI, there is essentially no variance in the PIB block T_g (ca. −65 °C, based on inflection point), with respect to DMAc swelling–drying, ionomer formation or subsequent silicate loading to these degrees. This suggests that the silicate component does not reside in the PIB phase because long range chain segmental mobility in these regions is not perturbed.

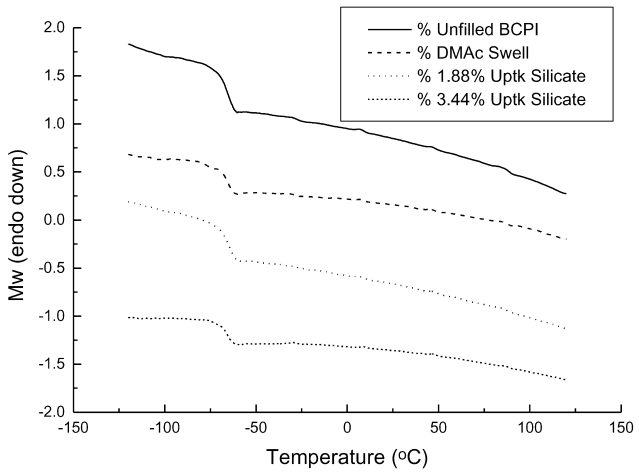

Fig. 6. Second scan DSC thermograms for an unfilled BCP, a corresponding Na^+BCPI, and two corresponding Na^+BCPI/silicate composites having indicated silicate uptakes for the samples described in the text. The curves have been vertically displaced for better viewing.

3.4. ^{23}Na solid state NMR spectroscopic investigations of ion clustering in a Na^+BCPI

^{23}Na SSNMR spectroscopy can probe the immediate chemical environment and mobility of Na^+ ions owing to the interaction of the Na nuclear quadrupole moment with local electric field gradients, in this case, gradients due to Coulombic fields around other Na^+ ions or polymer-affixed anions. As peaks shift to less negative values, interactions between Na^+ ions become weaker, so that this concept can be useful in determining whether Na^+ ions are isolated or exist in aggregates [18–26]. Here, isolated Na^+ ions are assumed to exist in electrostatically bound $-SO_3^-Na^+$ ion pairs in the dry state. The view of an 'aggregate' within the context of these BCPs must include Na^+ ions on the same PS block as well as on different PS blocks. This degree of ambiguity is compounded by the fact that the absolute size of these aggregates cannot be derived from this method. It should be mentioned that Weiss et al. [27] who studied similar sulfonated PS-*co*-(ethylene-*ran*-butylene)-*co*-PS materials, offered the idea that there are ion-rich regions within the PS domains

The spectra of the as cast, dry, and hydrated samples are shown in Fig. 7. The sharp resonance at ~10 ppm is attributed to isolated $Na^+SO_3^-$ groups, while the broad peak centered about −20 ppm for the as cast and dry samples is attributed to aggregated $SO_3^-Na^+$ ion pairs. These assignments are based on those made by Cooper and coworkers [22–25] and Moore and Gummaraju [28] who studied sulfonated PS ionomers. The small peak at about 0 ppm is attributed to hydrated, presumably dissociated Na^+ ions. The hydrated spectrum suggests that almost all of the Na^+ ions are solvent-separated, a condition that was discussed by Mauritz and Komoroski [29] with regard to the Na^+ form of hydrated vs. dry Nafion® sulfonate membranes.

3.5. AFM studies of composite morphology

We present a representative micrograph to illustrate the

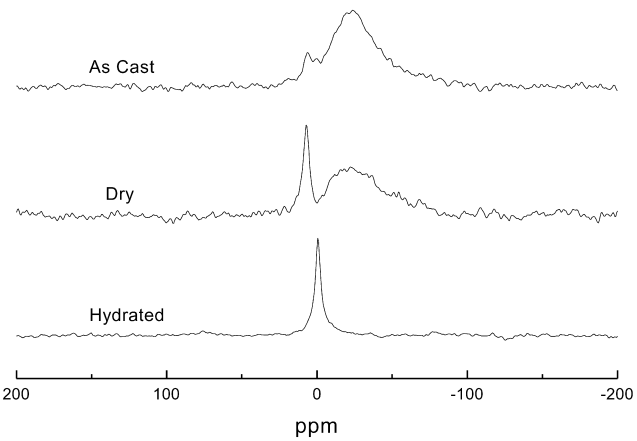

Fig. 7. ^{23}Na SSNMR spectra for the Na^+ form BCPI described in the text. The same sample was exposed to the different indicated conditions.

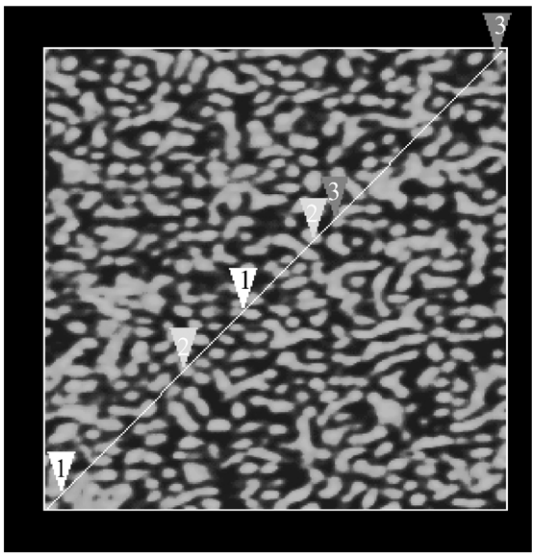

Fig. 8. AFM tapping mode/phase image of a 1 μm × 1 μm region, near the film surface, of the cross-section of the Na^+BCPI/(3.44 wt% silicate) composite described in the text. *Z*-range = 120°. The numbers on the arrows refer to positions in the sectional analysis profile seen in Fig. 10.

basic morphology that exists when the Na^+ form BCPI is used as the sol–gel reaction template. Fig. 8 is an AFM tapping mode/phase image of a 1 μm × 1 μm region located near the film surface of the cross-section of a Na^+BCPI/(3.44 wt%) silicate composite. The numbers on the arrows refer to positions on the graph in Fig. 9. This particular composite is based on a BCP for which M_w = 78.4 kg mol^{-1} and the PS composition is 28.5 wt% of which 12.8 mol% is sulfonated.

Phase separation exists on a scale of the order of tens-of-nanometers. The degree of order is less than that observed for hybrids based on the same BCPI in the $BTMA^+$ cation form for which the morphology consisted of distinct ordered arrays of hexagonally packed cylindrical rods [9]. The morphology seen in Fig. 8 lacks long range order associated with a crystalline array of scattering elements. Rather than straight rods, the minor phase elements are twisted and wormlike and are inefficiently packed.

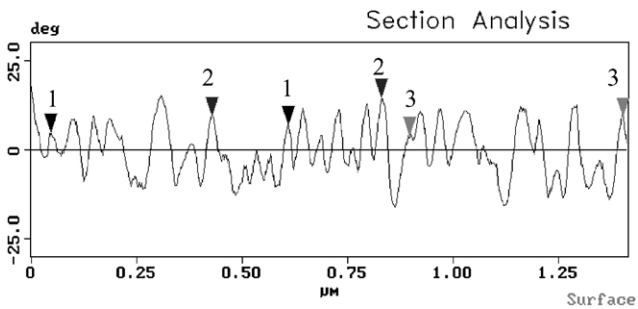

Fig. 9. Cross-sectional profile along the indicated diagonal for the tapping mode/phase AFM phase image. The *y*-axis is pixel intensity (expressed in degrees of phase angle) and the *x*-axis is horizontal distance (in μm) along the diagonal indicated in this figure. Numbers above the arrows were added for clarity.

A 'section analysis' of a 1 μm × 1 μm area of the phase image in Fig. 8 was conducted using the Digital Instruments Nanoscope™ software. An AFM micrograph is composed of pixels of different intensity, in this case, intensity being due to differences in phase. The lighter pixels correspond to PS domains and the darker pixels correspond to PIB domains. The straight line drawn diagonally across the micrograph traverses regions composed of dark as well as light pixels. Pixel intensity, when plotted against distance along the line can yield information regarding average inter-feature spacings. 'Features' refers to the light colored, irregularly shaped objects that constitute a minor phase. Three sets of marker arrows define three segments along the diagonal line. Each peak in the profile corresponds to a region of high pixel intensity, and therefore the PS component. Ten periods of intensity oscillation lie between each set of marker arrows and average domain spacing is obtained when the distance between the markers is divided by 10. The results for three different marker sets are averaged. For the data in Fig. 9, average domain spacing is 49.0 nm and the difference between the highest and lowest values for the three averages is 16 nm. While the spread in domain spacing is larger than those for highly ordered morphologies, this average can be useful in the interpretation of Bragg spacings that are derived from the broad and few SAXS peaks for these heterogeneous materials.

3.6. SAXS studies of morphology

The non-crystallinity-related SAXS peak present for random copolymer ionomers such as Surlyn®, sulfonated polystyrene and Nafion® is considered as evidence of phase separation in the sense of ionic aggregation [30]. In unmodified ABA BCPs, there is greater order with larger spacings in biphasic morphologies characterized by higher order SAXS reflections. The monotonic sequence of the ratio of peak *q*-position to that of the first (lowest angle) reflection reflects the symmetry of the minor phase array. The progression 1, $\sqrt{2}$, $\sqrt{3}$, $\sqrt{4}$,… corresponds to a body centered cubic array of spheres, 1, $\sqrt{3}$, $\sqrt{4}$, $\sqrt{7}$,… corresponds to hexagonally packed cylinders, and 1, 2, 3, 4,… corresponds to lamellae [31,32]. If sulfonate groups are added to the styrene blocks in styrene-*b*-[hydrogenated butadiene]-*b*-styrene polymers, there is an additional complication posed by the distribution of such ions (aggregated vs. uniformly dispersed) within the styrenic phase and perturbations of these ions on morphology [27]. It is suggested in Section 3.4 that the ions can exist in aggregates as well as in isolation within the blocks of the ionomers discussed here.

Figs. 10 and 11 are SAXS profiles for the series of Na^+BCPI samples having different levels of modification. Fig. 10(a) corresponds to an as cast Na^+BCPI film. Fig. 10(b) is the profile for a control sample that was first swollen in DMAc, the sol–gel reaction solvent, and then vacuum-dried at an elevated temperature. Fig. 11(a) and (b)

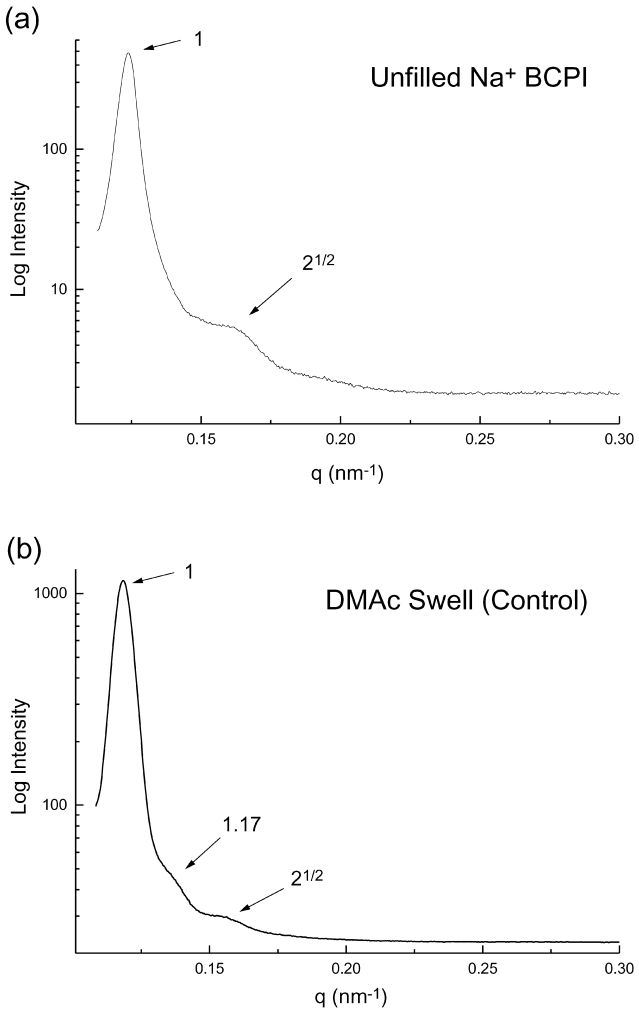

Fig. 10. (a) SAXS profile for an unfilled, as cast Na^+BCPI film having 28.5 wt% PS of which 12.8 mol% is sulfonated. (b) Same film as in (a), but sample was soaked in DMAc and subsequently dried in vacuum.

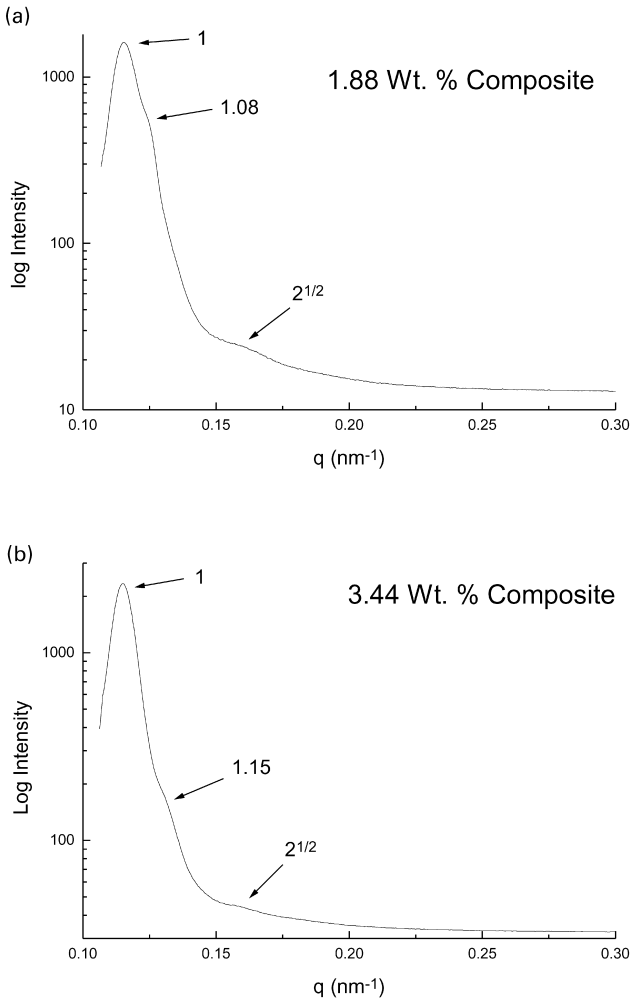

Fig. 11. (a) and (b), same Na^+BCPI film as in Fig. 10, but having indicated percent silicate.

are scattering profiles for in situ sol–gel modified Na^+BCPI films with different weight percent silicate uptakes. A summary of the relative positions of discernible peaks and the largest Bragg spacing (d_1) are in Table 1.

Given the small number of reflections, the degree of order in the unfilled BCPI is not as high as that in the unsulfonated BCP, nor is it as high as that seen in SAXS profiles for the same BCPI when benzyltrimethylamine is the counterion [33]. Perhaps, this is due to the stronger electrostatic interactions caused by Na^+ counterions, as might be inferred by the ^{23}Na SSNMR results. Each profile has peaks at relative positions 1 and $\sqrt{2}$ which is the beginning of the sequence for a spherical morphology although a hexagonal array of cylinders would be expected based on the styrene content of the parent BCP (28.5 wt%). All samples, except the as cast film, have an extra, presently inexplicable, intermediate peak which does not fit into the sequence for any of the common BCP morphologies. On comparing this evidence with that derived from the AFM studies, it is concluded that this nanocomposite possesses a 'frustrated' morphology.

Albeit of relatively low order, morphology is preserved throughout the sequence of BCPI modification and there is an increase in d_1 with increased silicate incorporation. The first peak shifts to smaller q with increased level of modification and d_1 increases from 50.7 to 54.6 nm. These values are similar to those obtained by the AFM section analysis. The increase in number of peaks from 2 to 3 is less affected by silicate incorporation as by swelling in DMAc

Table 1
SAXS data for indicated series of modified Na^+BCPI film materials

Description	First peak	q_1 (nm^{-1})	d_1 (nm)	Second peak	Third peak
Unfilled	1	0.1239	50.7	$1.32 \approx \sqrt{2}$	–
DMAc-treated	1	0.1184	53.1	1.2	$1.3 \approx \sqrt{2}$
1.88%	1	0.1154	54.4	1.1	$1.4 \approx \sqrt{2}$
3.44%	1	0.1150	54.6	1.2	$1.4 \approx \sqrt{2}$

Primary peak position (q_1) and corresponding Bragg spacing (d_1).

followed by drying. The concept of silicate nanostructures forming in/around PS domains is compatible with these results.

4. Conclusions

The PS blocks in elastomeric PS–PIB–PS BCPs were partially sulfonated using acetyl sulfate as a sulfonating reagent. Then, the sulfonic acid groups were converted to Na^+-sulfonate groups to form an ionomer. DMAc was used to selectively swell the ionic PS domains and the swollen films were immersed in reactive TEOS solutions. $(EtO)_{4-x}Si(OH)_x$ monomers permeated the film so that sol–gel reactions occurred within/around the ionic PS domains.

ESEM–EDS investigations of the Si elemental composition profile across the thickness direction of these films showed that a silicate component can indeed be incorporated within the interior of these Na^+BCPI films and that this composition profile depends on sample thickness.

DSC studies indicated that there is essentially no variance in the PIB block T_g with respect to ionomer formation or with respect to silicate loading of the ionomer at low levels. This suggests that the silicate component does not reside in the PIB phase because long range chain segmental mobility therein is apparently not perturbed.

^{23}Na SSNMR spectroscopy detected isolated $Na^+SO_3^-$ groups as well as aggregated $SO_3^-Na^+$ ion pairs for as cast and dry non-silicate containing ionomer samples. The spectrum for a hydrated sample suggests that almost all the Na^+ ions are solvent-separated and are most likely dissociated from the sulfonate anions. Future studies using this technique will include BCPI/silicate samples.

AFM analysis of the morphology of a composite demonstrated that phase separation exists, but that the degree of phase order is considerably less than that for hybrids based on the corresponding, earlier-studied, $BTMA^+$ ionomer. SAXS studies also indicate a frustrated morphology when Na^+ is the counterion. Both AFM and SAXS yielded an average domain spacing of around 50 + nm. Thus, based on this dimensional scale, these hybrids can indeed be classified as nanocomposites.

Acknowledgments

The authors gratefully acknowledge the support of the DOD EPSCoR program, administered by the Army Research Office, under grant DAAD19-99-1-0030. Acknowledgement is also made to Dr William Jarrett, Department of Polymer Science, University of Southern Mississippi, for his assistance in obtaining the NMR spectra.

References

[1] Mauritz KA. Mater Sci Engng 1998;C6:121.
[2] Juangvanich N, Mauritz KA. J Appl Polym Sci 1998;67:1799.
[3] Mauritz KA, Payne JT. J Membr Sci 2000;168:39.
[4] Young SK, Mauritz KA. J Polym Sci, Part B: Polym Phys 2001;39:1282.
[5] Siuzdak DA, Mauritz KA. J Polym Sci, Part B: Polym Phys 1999;37:143.
[6] Siuzdak DA, Start PR, Mauritz KA. J Appl Polym Sci 2000;77(13):2832.
[7] Mauritz KA, Jones CK. J Appl Polym Sci 1990;40:1401.
[8] Deng Q, Cable KM, Moore RB, Mauritz KA. J Polym Sci, Part B: Polym Phys Ed 1996;34:1917.
[9] Mauritz KA, Storey RF, Mountz DA, Reuschle DA. Polymer 2002; in press.
[10] Reuschle DA, Mountz DA, Mauritz KA, Brister LB, Storey RF, Beck Tan N. Am Chem Soc, Div Polym Chem Prepr 1999;40(2):713.
[11] Mountz DA, Beck Tan N, Storey RF, Mauritz KA. Am Chem Soc, Div Polym Chem Prepr 2000;41(1):273.
[12] Chen W, Feng H, Ye C. Polym J 1997;29(12):992.
[13] Hench LL, Ulrich DR, editors. Ultra-structure processing of ceramics, glasses and composites. New York: Wiley; 1984. p. 102.
[14] Storey RF, Chisholm BJ, Lee Y. Polym Engng Sci 1997;37(1):73.
[15] Brister LB. Doctoral Dissertation. The University of Southern Mississippi; 1999.
[16] Storey RF, Baugh DW, Choate KR. Polymer 1999;40:3083.
[17] Weiss RA, Sen A, Wills CL, Potick LA. Polymer 1991;32:1867.
[18] Komoroski RA, Mauritz KA. J Am Chem Soc 1978;100:7487.
[19] Samoson A. Chem Phys Lett 1985;119:29.
[20] Dickinson CL, MacKnight WJ, Connolly JM, Chien CW. Polym Bull 1987;17:459.
[21] Park JK, Park BK, Ryoo R. Polym Engng Sci 1991;31:873.
[22] O'Connell EM, Root TW, Cooper SL. Macromolecules 1994;27:5803.
[23] O'Connell EM, Root TW, Cooper SL. Macromolecules 1995;28:3995.
[24] O'Connell EM, Root TW, Cooper SL. Macromolecules 1995;28:4000.
[25] O'Connell EM, Peiffer DG, Root TW, Cooper SL. Macromolecules 1996;29:2124.
[26] Orler BE, Gummaraju RV, Calhoun BH, Moore RB. Macromolecules 1999;32:1180.
[27] Weiss RA, Sen A, Pottick LA, Willis CL. Polymer 1991;32(15):2785.
[28] Gummaraju RV, Moore RB. ACS Div Polym Chem, Polym Prepr 1998;39(1):387.
[29] Komoroski RA, Mauritz KA. In: Eisenberg A, Yeager HL, editors. Perfluorinated ionomer membranes. American Chemical Society Symposium Series; 1982. 180. chapter 7.
[30] Tant MR, Mauritz KA, Wilkes GL, editors. Ionomers: synthesis, structure, properties and applications. London: Blackie; 1997.
[31] Hashimoto T, Fetters LJ. Macromolecules 1993;26:5796.
[32] Hashimoto T, Sakurai S. Macromolecules 1993;26:485.
[33] Mountz DA, Beck Tan N, Storey RF, Mauritz KA. Am Chem Soc Polym Div Prepr 2000;41(1):273.